Molecular basis for nuclear accumulation and targeting of the inhibitor of apoptosis BIRC2

Adam Tencer, Yucong Yu, Sebastien Causse, Grant Campbell, Brianna Klein, Hongwen Xuan, Jessy Cartier, Mark Miles, Nitika Gaurav, Aymeric Zadoroznyj, et al.

Molecular basis for nuclear accumulation and targeting of the inhibitor of apoptosis BIRC2

Adam H. Tencer[1,8], Yucong Yu[2,8], Sebastien Causse[3,8], Grant R. Campbell[4,5,8], Brianna J. Klein[1], Hongwen Xuan[2], Jessy Cartier[3], Mark A. Miles[6], Aymeric Zadoroznyj[3], Tina A. Holt[1], Hong Wen[2], Christine J. Hawkins[6], Stephen A. Spector[4,7,*], Laurence Dubrez[3,*], Xiaobing Shi[2,*] and Tatiana G. Kutateladze[1,9,*]

[1]Department of Pharmacology, University of Colorado School of Medicine, Aurora, CO 80045, USA

[2]Department of Epigenetics, Van Andel Research Institute, Grand Rapids, MI 49503, USA

[3]Institut National de la Santé et de la Recherche Médicale (Inserm), LNC UMR1231, 21000 Dijon, France and Université de Bourgogne Franche-Comté, LNC UMR1231, 21000 Dijon, France

[4]Division of Infectious Diseases, Department of Pediatrics, University of California San Diego, La Jolla, CA 92093, USA

[5]Division of Basic Biomedical Sciences, Sanford School of Medicine, University of South Dakota, Vermillion, SD 57069, USA

[6]Department of Biochemistry and Chemistry, La Trobe Institute for Molecular Science, La Trobe University, Bundoora, VIC 3086, Australia

[7]Rady Children's Hospital, San Diego, CA 92123, USA

[8]Equal contribution

[9]Lead contact: Tatiana G. Kutateladze

*Correspondence: tatiana.kutateladze@cuanschutz.edu, xiaobing.shi@vai.org, laurence.dubrez@u-bourgogne.fr, saspector@health.ucsd.edu

Keywords: BIRC2, cIAP1, BIR domain, structure, histone, inhibitor

Abstract

The inhibitor of apoptosis protein (IAP) BIRC2 regulates fundamental cell death and survival signaling pathways. Aberrant activity of BIRC2 is associated with immunological diseases, inflammation, and cancer. Unlike other IAPs, BIRC2 can localize to and function in the nucleus through unknown mechanisms. Here, we show that BIRC2 accumulates in the nucleus via binding of its second and third BIR domains, $BIRC2_{BIR2}$ and $BIRC2_{BIR3}$, to histone H3 tail and report the crystal structure of the $BIRC2_{BIR3}$:H3 complex. RNA-seq analysis of cells in which the *BIRC2* gene is knocked out by CRISPR/Cas9 reveals that the genes involved in the interferon and defense response signaling and the cell cycle regulation are most affected by depletion of BIRC2. Overexpression of BIRC2 delays DNA damage repair and recovery of the cell cycle progression and extends the etoposide-induced G2/M cell cycle arrest. We describe the structural mechanism for targeting of $BIRC2_{BIR3}$ by a potent but biochemically uncharacterized small molecule inhibitor LCL161 and demonstrate that LCL161 disrupts the association of endogenous BIRC2 with H3 and readily stimulates cell death in cancer cells. We further show that LCL161 mediates degradation of BIRC2 in HIV-1 infected human CD4+ T cells. Our findings provide mechanistic insights into the nuclear accumulation of and blocking BIRC2.

Introduction

Human inhibitor of apoptosis (IAP) proteins are major regulators of apoptotic pathways and are implicated in inflammatory and innate immune signaling. Aberrant activities particularly of cellular IAPs (cIAPs) – cIAP1, also known as BIRC2, and cIAP2 – have been associated with cancer, inflammation and immunopathogenesis[1-3]. Acute or latent human immunodeficiency virus type 1 (HIV-1) infection increases the expression of IAPs[4] leading to the inhibition of HIV-1 transcription[5-7]. cIAPs contain three baculovirus IAP repeats (BIRs), a ubiquitin associating (UBA) domain, a CARD domain, and a RING finger (Fig. 1a). The second and third BIR repeats of cIAPs form complexes with caspases, whereas the RING finger of cIAPs functions as an E3 ubiquitin ligase, which mediates autoubiquitination and ubiquitination of protein substrates[8-10]. The anti-apoptotic activity of cIAPs is countered by IAP antagonists, such as second mitochondria-derived activator of apoptosis (Smac)[11-13]. The upregulation of IAPs has been shown to reduce autophagy through the ubiquitination of BECN1, inhibit apoptosis through the antagonization, ubiquitination and neddylation of caspases, and increase the ubiquitination of RIPK1[1,2,9,14]. The latter promotes pro-survival NF-κB signaling while also inhibiting the assembly of distinct RIPK1 complexes that regulate cell death. Beyond the regulation of apoptosis, cIAPs were found to promote cell proliferation, migration and invasion and mediate the cell cycle, chromosome segregation in mitosis, DNA damage response and transcription[15-20].

Unlike other IAP family members that are found primarily in the cytosolic fraction, BIRC2 can localize to the cell nucleus through an unknown mechanism[21,22]. Furthermore, because BIRC2 is overexpressed in response to HIV-1 infection and in various cancers, it has emerged as an attractive therapeutic target[23-28]. Among many cIAP targeting small molecule compounds developed in the past few years, LCL161, designed to mimic Smac, has received considerable attention[25]. LCL161 is characterized by favorable pharmacological properties and minor toxicity and is currently being investigated in many pre-clinical and phase I and phase II clinical studies[25,26]. It shows potent anti-cancer activity in at least two dozen tumor types and sensitizes

cancer cells to conventional chemotherapy with cisplatin and vincristine[25,26], yet our understanding of the biochemical mechanisms underlying the LCL161 effect is lacking.

Here, we show that BIRC2 engages with chromatin through binding to histone H3 tail and elucidate the mechanistic details and biological consequences of this engagement. We also describe the structural basis for targeting of BIRC2 by LCL161 and highlight the molecular mechanism by which LCL161 triggers cell death in cancerous and HIV-1-infected T cells.

Results and Discussion

BIRC2 recognizes histone tails

The association of BIRC2 with chromatin was originally observed in salt gradient fractionation of the isolated nuclei from SW480 cells and proximity ligation assay (PLA). Endogenous BIRC2 was detected in the nuclear fraction containing 0.3-0.5 M NaCl (Fig. 1b), and it was bound to histone H3 in PLA (Fig. 1c, d). The histone binding function of BIRC2 was substantiated by pulldown experiments using BIR domains of BIRC2 and histone peptides (Fig. 1e). The third BIR domain ($BIRC2_{BIR3}$) bound to the N-terminus of histone H3 (residues 1-22 of H3) but did not recognize other histones. The second BIR domain ($BIRC2_{BIR2}$) associated mostly with H3 and to a lesser extent with the N-termini of H4 and H2A, whereas the first BIR domain ($BIRC2_{BIR1}$) did not show histone binding activity. The histone selectivity, i.e. the strong binding to H3 and weaker binding to H4 and H2A, was maintained in the construct containing all three BIRs ($BIRC2_{3BIR}$), which represented a unique histone reader capable of recognizing all but H2B tails. To characterize the binding of BIRs in detail, we produced ^{15}N-labelled domains and monitored their interactions with the $H3_{1-12}$ (residues 1-12 of H3) peptide by NMR spectroscopy (Fig. 1f). ^{1}H,^{15}N HSQC (heteronuclear single quantum coherence) spectra of BIRs were recorded while the H3 peptide was added stepwise to the NMR samples. Large chemical shift perturbations (CSPs) in the spectra of $BIRC2_{BIR3}$ and $BIRC2_{BIR2}$ were induced by the peptide and indicated formation of the BIR-H3 complexes. CSPs were in the slow exchange regime on the NMR

timescale for $BIRC2_{BIR3}$ and the intermediate exchange regime for $BIRC2_{BIR2}$ and suggested tight binding to both domains. In agreement, a 400 nM binding affinity of $BIRC2_{BIR3}$ for the $H3_{1-12}$ peptide and a 720 nM binding affinity of $BIRC2_{BIR2}$ for the $H3_{1-12}$ peptide was measured in fluorescence assays (Fig. 1g, h and Suppl. Fig. 1). These K_d values were in the range of binding affinities of other histone binding modules[29-31], supporting the finding that BIRs are epigenetic readers with selectivity for H3.

Molecular mechanism for the $BIRC2_{BIR3}$ association with H3

To gain insight into the molecular basis for the recognition of the H3 tail, we co-crystallized $BIRC2_{BIR3}$ and $H3_{1-12}$ peptide and obtained a 1.8 Å resolution crystal structure of the $BIRC2_{BIR3}$:H3 complex (Fig. 1i-k and Suppl. Table 1). In the complex, $BIRC2_{BIR3}$ folds into a compact globular structure consisting of five short α-helices, a three-stranded anti-parallel β-sheet, and a zinc-binding cluster (Fig. 1i). The histone peptide is bound in a groove formed by the β3 strand, α3 helix and the β3-α3 loop. Analysis of the structure reveals an extensive network of hydrogen bonding, hydrophobic and electrostatic contacts that stabilize the complex. Ala1 of the H3 peptide occupies a highly negatively charged pocket lined by the side chains of E317, D320 and E325 of the protein (Fig. 1i, j). The N-terminal amino group of Ala1 of H3 is restrained through the hydrogen bonds with the carboxyl group of D320 and the backbone carbonyl group of C315 (Fig. 1k). The backbone carbonyl of Ala1 of H3 forms a hydrogen bond with the indolyl nitrogen atom of W329, whereas the backbone amino and carbonyl groups of Arg2 of H3 are involved in hydrogen bonding contacts with the backbone carbonyl and amino groups of R314. The sidechain ε-amino moiety of Lys4 donates a hydrogen bond to the carboxyl group of D303, and the backbone amino group of Lys4 is hydrogen bonded to the carbonyl oxygen atom of G312.

Overlay of the structures of $BIRC2_{BIR3}$ in complex with H3, Smac and caspase-9 reveals that these ligands occupy the same binding site of $BIRC2_{BIR3}$ (Suppl. Fig. 2). The position of the backbone and even various side chain atoms of the three bound to $BIRC2_{BIR3}$ sequences – ARTK of H3, AVPI of Smac, and ATPF of caspase-9 – is remarkably similar, despite the fact that only the first alanine residue is conserved. The deletion of Ala1/Arg2 in the histone H3 peptide (H_{3-33}) notably reduced binding of $BIRC2_{BIR2}$, $BIRC2_{BIR3}$ and $BIRC2_{3BIR}$ (Fig. 2a). Posttranslational modifications (PTMs), commonly found in histone H3, including methylation, acetylation and crotonylation of lysine residues, did not alter binding of BIRs, but methylation of Arg2 reduced binding of $BIRC2_{BIR3}$ to H3 (Suppl. Fig. 3). Yet, the most notable PTM-induced effect was caused by phosphorylation of Thr3, which abrogated binding of $BIRC2_{BIR3}$ but only slightly reduced binding of $BIRC2_{BIR2}$, as seen in pull down assays and NMR titration experiments (Fig. 2b-d). The structure of the $BIRC2_{BIR3}$-H3 complex provides an explanation to the observed sensitivity of $BIRC2_{BIR3}$. Thr3 is in close proximity to the negatively charged Ala1-binding pocket, therefore the presence of the negatively charged phosphate group should lead to electrostatic repulsion. Additionally, phosphorylation of Thr3 is unfavorable due to steric clashes with the bulky side chain of W329, the position of which is fixed as it forms the hydrogen bond with the carbonyl group of Ala1 (Fig. 1k). In contrast, $BIRC2_{BIR2}$ contains less bulky H243 in place of W329, which may tolerate Thr3 phosphorylation, especially if it is at least partially protonated.

BIRs mediate histone and DNA binding functions of BIRC2

The importance of caging Ala1 of H3 for the interaction of $BIRC2_{BIR3}$ and $BIRC2_{BIR2}$ with the histone tail was corroborated by mutagenesis. We generated D320A and E325A mutants of $BIRC2_{BIR3}$ and the corresponding D234A and E239A mutants of $BIRC2_{BIR2}$ and tested them by NMR (Fig. 2e-g) and pulldown assays (Fig. 2h, i). As shown in Fig. 2e-i, substitution of the negatively charged residues with an alanine abrogated binding of individual $BIRC2_{BIR2}$ and

153 BIRC2$_{BIR3}$ to H3 and H3T3ph, however, mutations in both domains (D234A/D320A) concurrently
154 were needed to disrupt binding of the triple BIRC2$_{3BIR}$ (Fig. 2i). Notably, the BIRC2$_{BIR1}$ sequence
155 contains positively charged lysine residues in place of E317 and E325 in BIRC2$_{BIR3}$ (Fig. 2j),
156 which likely accounts for the inability of BIRC2$_{BIR1}$ to recognize H3 (Fig. 1e, f). As genetic
157 mutations within BIRC2$_{BIR2}$ and BIRC2$_{BIR3}$ have been identified in various cancers, we also
158 generated a set of cancer-relevant mutants and examined their histone binding activities in
159 pulldown assays (Suppl. Fig. 4). The cancer relevant mutations in BIRC2$_{BIR3}$, including L313F,
160 W316R and D320N, eliminated binding to H3, and the BIRC2$_{BIR2}$ H243W mutant lost its ability to
161 tolerate Thr3 phosphorylation, pointing to a potential role of the BIR-H3 interactions in
162 oncogenesis.
163 A number of chromatin-binding proteins have been shown to associate with both histone
164 tails and DNA[32]. We tested whether BIRC2 has a DNA binding function using electrophoretic
165 mobility shift assays (EMSA). Increasing amounts of BIRC2$_{BIR1}$, BIRC2$_{BIR2}$ and BIRC2$_{BIR3}$ were
166 incubated with 601 DNA, and the reaction mixtures were resolved on a native polyacrylamide
167 gel (Fig. 2k-m). A shift of the free 601 DNA indicated formation of the BIRC2$_{BIR1}$:DNA complex,
168 whereas no DNA binding activity was detected for BIRC2$_{BIR2}$ and BIRC2$_{BIR3}$. These data imply
169 that BIRC2 can bivalently engage with chromatin through binding of BIRC2$_{BIR2}$ and BIRC2$_{BIR3}$ to
170 H3 and binding of BIRC2$_{BIR1}$ to DNA.
171
172 **BIRC2 regulates the cell defense and cell cycle signaling**
173 To identify the genes regulated by BIRC2, we knocked out endogenous BIRC2 in the MCF-7
174 breast cancer cell line using CRISPR/Cas9 and two sgRNAs targeting BIRC2 (Suppl. Fig. 5)
175 and extracted total RNA for next generation sequencing. RNA-seq analysis identified 526 genes
176 that were upregulated and 443 genes downregulated in the cells expressing BIRC2 sgRNAs
177 (Fig. 3a and Suppl. Table 2). Gene Ontology (GO) analysis revealed that the genes involved in
178 the interferon and defense response signaling pathways and the cell cycle regulation were most

affected by the depletion of BIRC2 (Fig. 3b and Suppl. Table 3). In support of GO analysis, in the interferon-γ (IFN-γ) stimulated *ex-vivo* differentiated normal peripheral blood monocytes, inhibition of IAPs with the XIAP inhibitor embelin led to an increase of interleukin-6 (IL-6), as observed in the cytokines antibody array (Fig. 3c). We also investigated DNA damage response and the cell cycle regulation in BIRC2-overexpressing HeLa cells (Fig. 3d-f). Cells were briefly treated with a low concentration of etoposide until the DNA damage marker γH2AX was detected (Fig. 3e, f) and then cultured in a drug-free medium to allow for DNA repair and the restoration of the normal cell cycle. Overexpression of BIRC2 delayed the DNA damage repair judging by the persistent level of γH2AX in western blot and flow cytometry assays, even 6 h after the drug removal (Fig. 3e, f). The delay in the DNA damage repair was further corroborated by a flow cytometry analysis of the cell cycle (Fig. 3g). Overexpression of BIRC2 delayed the recovery of the cell cycle progression and extended the etoposide-induced G2/M cell cycle arrest (Fig. 3g, h).

LCL161 binds to $BIRC2_{BIR3}$ and $BIRC2_{BIR2}$ but not to $BIRC2_{BIR1}$

Among several Smac mimetic compounds developed in the past few years, LCL161 (Fig. 4a) displays one of the most promising anti-proliferation and bioavailability properties[25,26,33]. While therapeutic potency of LCl161 has been established in pre-clinical and clinical studies, little is known about its binding mechanism. To better understand the molecular basis underlying its inhibitory activity, we investigated how LCL161 interacts with each BIR domain of BIRC2. LCL161 was titrated into NMR samples of individual ^{15}N-labelled $BIRC2_{BIR1}$, $BIRC2_{BIR2}$ and $BIRC2_{BIR3}$ while ^{1}H,^{15}N HSQC spectra were recorded, processed and overlayed (Fig. 4b-d). LCL161 caused CSPs in the spectra of $BIRC2_{BIR3}$ and $BIRC2_{BIR2}$ but not in the spectrum of $BIRC2_{BIR1}$, revealing that $BIRC2_{BIR3}$ and $BIRC2_{BIR2}$ but not $BIRC2_{BIR1}$ are direct targets of the compound. The K_d values, measured by tryptophan fluorescence, were found to be 490 nM for $BIRC2_{BIR3}$ and 2.2 μM for $BIRC2_{BIR2}$ (Fig. 4e, f).

The mechanistic details of the interaction with LCL161 were obtained from the crystal structure of the $BIRC2_{BIR3}$:LCL161 complex (Fig. 4g, h and Suppl. Table 1). The complex is stabilized by a large set of hydrogen bonds. These include contacts between the side chain carboxyl groups of D320 and E325 and the methylamino group of LCL161 and between the carbonyl group of alanine in LCL161 and the indolyl moiety of W329. The amino group and the carbonyl group of cyclohexylglycine in LCL161 are hydrogen bonded with the backbone carbonyl group and the amino group of R314, respectively. Additionally, the side chain guanidino group of R314 is near the *p*-fluorobenzoyl group in LCL161, whereas the thiazole ring of LCL161 is in close proximity to G312. LCL161 lays in the histone H3-binding site, ideally tracing the geometry of the H3 peptide (Fig. 4i, j), and overlays with GDC0152, another BIRC2 inhibitor (Suppl. Fig. 6).

LCL161 disrupts binding of BIRC2 to H3 and stimulates cell death

The impact of LCL161 on endogenous BIRC2 was tested in colon adenocarcinoma SW480 cells. As shown in Figures 5a and 5b, treatment of the cells with LCL161 disrupted the association of BIRC2 with histone H3 in PLA (Fig. 5a, b). This result can be attributed to the binding of LCL161 to $BIRC2_{BIR3}$ and $BIRC2_{BIR2}$, as incubation of the isolated GST-tagged $BIRC2_{BIR3}$ and $BIRC2_{BIR2}$ with LCL161 abolished binding of $BIRC2_{BIR3}$ to the H3 peptide and decreased binding of $BIRC2_{BIR2}$ in pulldown experiments (Fig. 5c). Western blot analysis of BIRC2 following the treatment of SW480 cells with LCL161 for 1 hr showed that LCL161 induces BIRC2 degradation (Fig. 5d). LCL161 treatment of IFN-γ stimulated *ex-vivo* differentiated normal human peripheral blood monocytes led to an increase in IL-6 and RANTES expression, supporting the cytokines antibody arrays data (Fig. 3c) and BIRC2 degradation (Fig. 5e-g).

To explore the effect of LCL161 on pro-survival function of BIRC2, we monitored cell survival following treatment with LCL161, tumor necrosis factor α (TNFα), or both in a

colorimetric 3-(4,5-dimethylthiazol-2-yl)-2,5-diphenyltetrazolium (MTT) assay. Consistent with its ability to divert tumor necrosis factor receptor 1 (TNFR1) signaling toward cell death pathways, LCL161 sensitized murine embryonic fibroblasts (MEFs) and human glioma LN18 cells to killing by TNFα (Fig. 5h, i).

LCL-161 mediates BIRCs degradation in HIV-1-infected CD4+ T cells

The mechanism by which LCL161 promotes cell death was examined in *in vitro* HIV-1 infected human CD4+ T cells (HIV-T_{CM}). As identified previously, these HIV-T_{CM} have increased expression of BIRC2 and BIRC3 (cIAP2), the tumor necrosis factor (TNF) receptor superfamily (TNFRSF) death receptor FAS, and both membrane-bound and soluble FAS ligand (FASLG) compared with T_{CM} (Fig. 5j)[34,35] and the majority express the lineage markers CD45RO, CD62L, CCR7 and CD27 while not expressing high levels of activation (HLA-DR and CD25) or cellular proliferation (MKI67) markers after 30 d culture with IL-7 (Suppl. Fig. 7). Under physiologic conditions, the interaction of TNFRSF with its cognate ligand leads to receptor trimerization and the recruitment of FADD and caspase-8 to form a prominent death inducing signaling complex (DISC). IAPs can inhibit this effect through the post-translational ubiquitination of RIPK1 which activates canonical NF-κB pro-survival signaling pathways[36,37]. In cells with high expression of FAS and FASLG, loss of IAPs can result in the deubiquitination and autophosphorylation of RIPK1 at Ser^{166} that activates and increases RIPK1 recruitment to the FAS DISC alongside FADD, caspase-8 and cFLIP isoforms[38,39]. As the activation of FAS-induced apoptosis is known to be inhibited by IAPs, and FAS, FASLG, BIRC2, and BIRC3 are upregulated in HIV-T_{CM}, we treated HIV-T_{CM} and uninfected T_{CM} with LCL161. LCL161 induced the rapid degradation of BIRC2 and BIRC3 in both HIV-T_{CM} and the uninfected cells (Fig. 5k). This correlated with the deubiquitination and Ser^{166} phosphorylation, and thus activation of RIPK1 (Fig. 5k, l). We then examined the FAS DISC using co-immunoprecipitation for FAS. We readily detected the association of FADD, pro-caspase-8, activated caspase-8, RIPK1 (total, Ser^{166} phosphorylated,

and the cleaved form [p39]), $cFLIP_S$, and the p43 fragment of $cFLIP_L$ with FAS in HIV-T_{CM} after LCL161 treatment (Fig. 5k), whereas FADD, $cFLIP_S$, and Ser^{166} phosphorylated RIPK1 did not associate with FAS in the LCL161 treated T_{CM}.

The formation of the FAS DISC in HIV-T_{CM} correlated with the cleavage of caspase-3, the proteolysis of poly(ADP-ribose) polymerase 1 (PARP1) (Fig. 5m), an increase in cytoplasmic histone-associated DNA fragments (mono- and oligonucleosomes) (Fig. 5n), the translocation of phosphatidylserine from the inner to the outer leaflet (extracellular side) of the plasma membrane, permeabilization of the plasma membrane (Suppl. Fig. 8), and an increase in lactate dehydrogenase release from HIV-T_{CM} (Fig. 5n) but not in the uninfected cells, indicating that the cleavage of pro-capsase-8 within the FAS DISC resulted in the execution of apoptosis in the HIV-T_{CM}. This suggests that although RIPK1 was cleaved and $cFLIP_S$ was recruited to the FAS DISC, it was insufficient to prevent LCL161-mediated cell death[40]. In agreement with previous studies, a specific increase in HIV-T_{CM} cell death was not accompanied by an increase in HIV-1 p24 antigen release from infected cells (Suppl. Fig. 7c-d)[6,41]. To confirm a role for the LCL161-mediated degradation of BIRC2 in the observed cell death, we performed RNAi for *BIRC2* (Suppl. Fig. 9a-b), which resulted in the death of HIV-T_{CM} but not T_{CM} (Suppl. Fig. 9c). Collectively, these data demonstrate that the presence of BIRC2 inhibits FAS-mediated cell death of HIV-T_{CM}, and that the LCL161-mediated degradation of BIRC2 in HIV-T_{CM} leads to the assembly of the FAS DISC and subsequent cell death.

In conclusion, in this study we elucidate a mechanism by which BIRC2 localizes to the cell nucleus. We found that BIRC2 engages with chromatin in a multivalent manner: while its $BIRC2_{BIR2}$ and $BIRC2_{BIR3}$ domains robustly recognize histone H3 tail, $BIRC2_{BIR1}$ binds to DNA. We show that the nuclear pool of BIRC2 regulates a large set of the genes involved in the interferon and defense response signaling pathways and the cell cycle regulation. In support, immunoprecipitation and flow cytometry assays demonstrate that BIRC2 negatively regulates the DNA damage repair and the recovery of the cell cycle progression and extends the

etoposide-induced G2/M cell cycle arrest. The crystal structure of $BIRC2_{BIR3}$ in complex with a small molecule inhibitor LCL161 along with binding affinities of $BIRC2_{BIR2}$ and $BIRC2_{BIR3}$ toward LCL161 provide mechanistic insights into the inhibition of BIRC2, which is instrumental in the development of a new generation of Smac-derived inhibitors of IAPs with the goal to kill cancer and HIV-infected cells.

Data availability

Coordinates and structure factors have been deposited in the Protein Data Bank under accession numbers 7TRL and 7TRM. All other relevant data supporting the key findings of this study are available within the article, its Supplementary Information or from the corresponding authors upon reasonable request. Source Data are provided with this paper.

Code availability

This paper does not report original code.

Acknowledgements

This work was supported in part by grants from the NIH: GM125195, GM135671, HL151334, CA252707 and AG067664 to T.G.K., CA204020 to X.S., MH128021 to G.R.C., NS104015 to S.A.S. and CA255506 to H.W., and the International Maternal Pediatric Adolescent AIDS Clinical Trials Network (impaactnetwork.org) to S.A.S. Overall support for the International Maternal Pediatric Adolescent AIDS Clinical Trials (IMPAACT) Network is provided by the National Institute of Allergy and Infectious Diseases of the NIH under award numbers UM1AI068632 (IMPAACT LOC), UM1AI068616 (IMPAACT SDMC), and UM1AI106716 (IMPAACT LC), with co-funding from the Eunice Kennedy Shriver National Institute of Child Health and Human Development and the National Institute of Mental Health. The content is

solely the responsibility of the authors and does not necessarily represent the official views of the NIH.

Author contributions

A.H.T., Y.Y., S.C., G.R.C., B.J.K., H.X., J.C., M.A.M., A.Z. and T.A.H. performed experiments and together with H.W., C.J.H., S.A.S., L.D., X.S. and T.G.K. analyzed the data. A.H.T. and T.G.K. wrote the manuscript with input from all authors.

Conflict of interest

The authors declare no competing interests.

Online Methods

Cell culture

Human HeLa and SW480 cells were purchased from ATCC and cultured in Dulbecco's modified Eagle medium (DMEM) (Cellgro) supplemented with 10% fetal bovine serum (FBS) (Sigma), 2 mM L-glutamine and 100 U ml^{-1} penicillin/streptomycin. Human MCF-7 and LN18 cells and murine embryonic fibroblasts were cultured in DMEM with high glucose (Invitrogen; CA, USA) supplemented with 10% FBS (Sigma or Scientifix Life; VIC, Australia) and cells maintained at 37 °C in air supplemented with 5% CO2. HIV-1 was prepared and infectivity calculated as previously described[35]. Whole blood was drawn from HIV-1-seronegative healthy male and female volunteers, ages between 18 and 65 years, at UC San Diego Health Sciences using protocols approved by the Human Research Protections Program of the University of California San Diego in accordance with the requirements of the Code of Federal Regulations on the Protection of Human Subjects (45 CFR 46 and 21 CFR 50 and 56). All volunteers gave written informed consent prior to their participation, all samples were de-identified, and donors remained anonymous. Peripheral blood mononuclear cells (PBMC) were isolated from whole

blood by density gradient centrifugation over Ficoll-Paque Plus (GE Healthcare) and HIV-1 infected, resting CD4+ T cells (HIV-T_{CM}) were prepared from these PBMC and characterized as previously described[35]. Briefly, CD4+ T cells were isolated from PBMC using the CD4+ T cell isolation kit (Miltenyi Biotec, Cat# 130-096-533) and incubated for 48 h in GM (RPMI 1640 supplemented with 10% [vol/vol] heat-inactivated FBS, 50 µM 2-sulfanylethan-1-ol [both Sigma], 100 µM non-essential amino acids, 1 mM sodium pyruvate, 0.1 mg/mL streptomycin, 100 U/mL penicillin [all Gibco]) supplemented with 29 nM CCL19 (R&D Systems) before infection with 0.4 multiplicity of infection HIV-1_{NL4-3} (obtained from Malcolm Martin via the NIH HIV Reagent Program and prepared and titered as previously described[35] for 3 h. Cells were washed then plated at 5 × 10^5 cells/mL in GM supplemented with 250 ng/mL staphylococcal enterotoxin B (Sigma) and 25 U/mL IL-2 (Roche) and cultured for 3 d in 5% CO_2 at 37 °C. Cells were then washed and resuspended at 5 × 10^5 cells/mL in GM supplemented with 25 U/mL IL-2 and cultured at 5% CO_2 at 37 °C. Every 2-3 days, cell concentration was adjusted back to 5 × 10^5 cells/mL with 25 U/mL IL-2-containing GM and supernatant HIV-1 p24 release was monitored using the Perkin Elmer Alliance HIV p24 antigen ELISA. After 12 days memory CD4+ T cells were isolated by negative selection using a memory CD4+ T cell isolation kit (Miltenyi Biotec, Cat# 130-091-893). Memory CD4+ T cells were then cultured in RPMI 1640 supplemented with 10% (vol/vol) heat-inactivated FBS, 0.1 mg/mL streptomycin, 100 U/mL penicillin, and 1 ng/mL IL-7 (R&D Systems) for 30 d at 37 °C, 5% CO_2. Phenotyping and phytohemagglutinin-M (PHA; Sigma, Cat# L8902) inducible virus was assessed by flow cytometry, and quantification of HIV-1 integrated DNA was performed using a previously described nested Alu-LTR quantitative PCR (qPCR) assay[35]. LCL161 was obtained from Selleck Chemicals. Cell cytotoxicity was calculated using a lactate dehydrogenase (LDH) release assay according to the manufacturer's protocol (Takara Bio).

Protein expression and purification

The human BIRC2 BIR domains BIR1 (aa 37-123), BIR2 (aa 175-260) and BIR3 (aa 261-346) were cloned into pGEX 6p-1 vectors. All constructs were expressed in *Escherichia coli* BL21(DE3) RIL cells in ^{15}N-labled M9 minimal media or LB media supplemented with 50 μM $ZnCl_2$. Cultures were grown to an OD_{600} of 0.8 and induced with 0.5 mM IPTG for 18 hours at 16 °C. Bacteria were harvested by centrifugation and lysed by sonication. GST-tagged proteins were purified on Pierce glutathione agarose beads (Thermo Scientific) using first 20 mM Tris-HCl (pH 7.5), 500 mM NaCl, 0.5% Triton X-100 and 2 mM DTT buffer, and then 20 mM Tris-HCl (pH 7.5), 150 mM NaCl, and 2 mM DTT buffer. The GST-tag was cleaved with PreScission protease overnight at 4 °C. Proteins were further purified by size exclusion chromatography (SEC) and concentrated in Millipore concentrators (Millipore). For crystallographic studies of BIR3 and LCL-161, 20 mM Bis-Tris Propane (pH 7.5), 150 mM NaCl and 2 mM DTT was used in SEC.

Chromatin fractionation

SW480 cells were lysed in 10 mM HEPES pH 7.8 buffer, supplemented with 10 mM KCl, 1.5 mM $MgCl_2$, 0.34 M sucrose, 0.2% (v/v) NP-40, 10% (v/v) glycerol and protease inhibitors (Complete protease inhibitor cocktail tablet, Merck, 11697498001), and lysates were centrifuged. The nuclear fraction (pellet) was suspended in 3 mM EDTA buffer, supplemented with 0.2 EGTA and protease inhibitors, and centrifuged to separate supernatant (nucleoplasm) from the pellet. The pellet was successively subjected to gradient salt extraction with increasing concentrations of NaCl (0.1 M to 0.7 M) in 50 mM Tris buffer supplemented with 0.05% NP-40. Proteins of nucleoplasm and chromatin-associated fractions were then quantified and subjected to western blot analysis.

PLA

SW480 cells grown on No. 1.5 coverslips were fixed using 4% PFA in phosphate-buffered saline for 10 min at room temperature. Cells were permeabilized by chilled methanol at -20 °C for 10 min. The PLA was carried out using Duolink protocol and anti-BIRC2 (Atlas Antibodies, HPA005513), anti-histone H3 (Cell Signaling Technologies, 14269), anti-rabbit plus (Sigma-Aldrich, DUO92002) and anti-mouse minus (Sigma-Aldrich, DUO92004) PLA probes and PLA detection kit orange (Sigma-Aldrich, DUO92007) in the presence or absence of 10 µM LCL161. Microscopy images were acquired using a Zeiss Axio Imager 2 (Zeiss GmBH) equipped with ×20 0.46NA, ×40 0.6NA, and ×63 1.45 NA Plan Apochromatic objectives, and an mRM4 CCD camera. Illumination was provided by an HXP120 metal halide lamp (Zeiss GmBH). Filter sets used were 49 HE (DAPI; 488049-0000), 38 HE (Alexa488, 489038-0000) and 43 HE (Alexa568, 489043-0000). Image analysis was carried out using the ICY software (http://icy.bioimageanalysis.org), on 10 randomly taken fields (based on DAPI). Nuclei were segmented using the Active Contour plugin on DAPI signal; PLA were detected using the Spot Detector plugin. Fluorescence signals were measured in maximal projections of unmodified images. Western blotting of endogenous BIRC2 was performed before and after the treatment of SW480 cells with 10 µM LCL161 for 1 hour. SW480 cells were lyzed in RIPA buffer (50 mM Tris HCl pH 8, 150 mM NaCl, 1% NP-40, 0.5% sodium deoxycholate, 0.1% SDS, supplemented with a protease and phosphatase inhibitor cocktail). Anti BIRC2 and β-actin peroxidase conjugated antibodies were from R&D system (Cat# AF8181) and Sigma-Aldrich (Cat# 3854).

IFN-γ stimulation

Human peripheral blood monocytes were obtained from healthy donors with informed consent, purified and differentiated *ex vivo* into macrophages as previously described[42]. Macrophages were then stimulated by 100 UI/mL IFN-γ for 24 hrs with or without 10 µM embelin (Sigma-Aldrich) or 10 µM LCL161 in RPMI 1640 medium (Lonza), 10% fetal calf serum (Lonza). The supernatants were analyzed for the cytokines content by an antibody array (RayBiotech)

following the manufacturer protocol. The cytokines arrays were performed in duplicate. The arrays include: positive control, positive control, negative control, negative control, GCSF, GM-CSF, GRO, GRO-α, IL-1^{α}, IL-2, IL-3, IL-5, IL-6, IL-7, IL-8, IL-10, IL-13, IL-15, IFN-γ, MCP-1, MCP-3, MIG, RANTES, TGF-β, TNF-α, TNF-β, and positive control. IL-6 and RANTES expression were quantified by RT-qPCR as previously described[42]. Western blotting of endogenous BIRC2 was performed before and after the treatment of macrophages with 10 μM LCL161 for 24 hours as above.

DNA damage assay

HeLa cells were transfected with the pCI or pCI-BIRC2 vectors using JetPEI (Plyplus transfection, Ozyme). Cells were then treated with 1 μM etoposide for 3 hours, washed and cultured for 0 to 48 hours in a drug-free medium. DNA damage was evaluated by western-blot and immunofluorescence analysis of γH2AX using anti-phospho-H2AX (Ser139) (Millipore # DAM1546024, Merckmillipore). For immunofluorescence, cells were fixed using 4% PFA in PBS for 10 min, washed, permeabilized for 10 min with 100% methanol at -20°C and washed again. Nonspecific binding was blocked by 3% bovine serum albumin (BSA) for 1 hr. Samples were then incubated overnight with anti-γH2AX, washed four times, incubated with anti-rabbit Alexa Fluor 660 for 1 hr at room temperature, rinsed in water and analyzed on BD KSR II flow cytometer (BD Biosciences) (excitation: 488 nm laser light, detection: bandpass filter 620/20). For the cell cycle analysis, cells were fixed in cold 70% ethanol for 30 min, washed, treated with ribonuclease and stain with propidium iodide solution (25 μg/mL) prior to flow cytometry analysis (excitation: 488 nm laser light, detection: bandpass filter 620/20).

NMR experiments

NMR experiments were performed at 298K on a Varian INOVA 600 MHz spectrometer equipped with a cryogenic probe. The NMR samples contained 0.1 mM uniformly ^{15}N-labeled

wild-type or mutated BIR domains of BIRC2 in 20 mM Tris-HCl (pH 7) buffer supplemented with 150 mM NaCl, 5 mM DTT and 10% D_2O. Binding was characterized by monitoring chemical shift changes in ^{1}H,^{15}N HSQC spectra of the proteins induced by the addition of histone peptides (aa 1-12 of H3, synthesized by Synpeptides) or LCL-161.

Fluorescence spectroscopy

Sectra were recorded at 25 °C on a Fluoromax-3 spectrofluorometer (HORIBA). The samples containing 1 μM BIR domains of BIRC2 (in 20 mM Tris (pH 6.8), 150 mM NaCl and 1 mM DTT buffer) and progressively increasing concentrations of peptides or LCL161 were excited at 295 nm. Emission spectra were recorded between 330 and 360 nm with a 0.5 nm step size and a 1 s integration time. The K_d values were determined using a nonlinear least-squares analysis and the equation:

$$\Delta I = \frac{\Delta I_{max}\left(([L] + [P] + K_d) - \sqrt{([L] + [P] + K_d)^2 - 4[P][L]}\right)}{2[P]}$$

where [L] is concentration of the peptide or inhibitor, [P] is concentration of the protein, ΔI is the observed change of signal intensity, and ΔI_{max} is the difference in signal intensity of the free and bound states of the protein. K_d values were averaged over three separate experiments, and error was calculated as the standard deviation between the runs.

X-ray crystallography

The BIR3 domain of human BIRC2 (residues 261-346) was concentrated to 10 mg/ml and incubated on ice in a 1:1.2 molar ratio with either the H3 peptide (aa 1-12) or LCL-161 for 1 h. Crystals of the $BIRC2_{BIR3}$:H3 complex were grown using the sitting-drop vapor diffusion method at 18 °C by mixing equal volumes of protein solution with well solution composed of 0.1 M SPG buffer (2:7:7 molar ratio of succinic acid:sodium dihydrogen phosphate: glycine) pH 7.0,

supplemented with 25% PEG 1,500. Crystals of the $BIRC2_{BIR3}$:LCL161 complex were grown at 4 °C using the sitting-drop vapor diffusion method in 0.1 M Bis-Tris Propane (pH 7.5), 0.2 M Sodium Citrate, and 20% PEG3350. X-ray diffraction data were collected from single crystals on the CU Anschutz Medical Campus X-ray crystallography core facility Rigaku Micromax 007 high-frequency microfocus X-ray generator equipped with a Pilatus 200K 2D area detector. The phase solutions for the $BIRC2_{BIR3}$:H3 (Phenix) and $BIRC2_{BIR3}$:LCL161 (CCP4) complexes were obtained by molecular replacement using the $BIRC2_{BIR3}$ structure (PDB ID: 3D9T with the peptide, solvent and the zinc ion removed) as a search model. Indexing and scaling was completed using HKL3000. Manual model building was performed using Coot [43], and the structure was refined using Phenix[44]. The final structure was verified on the PDB validation server. The X-ray diffraction and structure refinement statistics are summarized in Supplementary Table 1.

Peptide pulldown assays

1 µg biotinylated histone peptides (synthesized by CPC scientific) with different modifications were incubated with 1 µg GST-fused BIRC2 BIR domains in binding buffer (50 mM Tris-HCl pH7.5, 300 mM NaCl, 0.1% NP-40, and 1 mM PMSF) overnight with rotation at 4 °C. Streptavidin magnetic beads (Pierce) were added to the mixture, and the mixture was incubated for 1 h with rotation at 4 °C. The beads were then washed three times using a magnetic stand and the bound proteins were analyzed using SDS-PAGE and Western blotting. Anti GST antibodies were from Santa Cruz (Cat# sc-459, AB_631586).

RNA-seq

Total RNAs were extracted from MCF7 cells by RNeasy Plus Mini Kit (QIAGEN, Cat. 74136). Illumina NovaSeq 6000 were used for generating polyA-plus 50 bp pair-end reads. Fastq reads were mapped to hg38 human genome by HISAT2 (v2.1.0)[45] with -k 1. DEGs were calculated by

edgeR (v3.16.5)[46] with Exact test model (FDR<0.05). GO term enrichment was done by DAVID 6.8[47]. Anti GAPDH antibodies were from Santa Cruz (sc-32233, RRID:AB_627679), and anti BIRC2 antibodies were from Abcam (Cat# ab108361, RRID:AB_10862855).

EMSA

EMSAs were performed by mixing increasing amounts of BIR domains of BIRC2 with 0.25 pmol of 601 DNA/lane in 25 mM Tris-HCl pH 7.5, 150 mM NaCl and 0.5 mM ethylenediaminetetraacetic acid (EDTA) in a 10 µL reaction volume. Reaction mixtures were incubated at room temperature for 10 min (2 µl of loading dye was added to each sample) and loaded onto a 5% native polyacrylamide gel. Electrophoresis was performed in 0.2x Tris-borate-EDTA (TBE) at 80-100 V on ice. The gels were stained with SYBR Gold (Thermo Fisher Sci) and visualized by Blue LED (UltraThin LED Illuminator-GelCompany).

MTT assays

Two thousand MEF or LN18 cells were seeded into wells of 96 well plates. Equal volumes of media containing LCL161 and/or TNFα were added to the cells and incubated for 24 h. Tetrazolium (MTT) reduction by viable cells to produce formazan crystals was quantitated as a measure of survival[48].

Flow cytometry

1×10^5 CD4+ T cells were harvested, washed in phosphate buffered saline (PBS) supplemented with 1 mg/mL bovine serum albumin and 100 µg/mL NaN_3 (FACS buffer) and stained with the following fluorescently conjugated antibodies in FACS buffer for 30 mins at 4 °C: allophycocyanin (APC)-eFluor 780 conjugated anti-CD3 (Cat# 47-0036-41, RRID:AB_10718679) or isotype control IgG (Cat# 47-4714-80, RRID:AB_1271993), eFluor 450 conjugated anti-CD4 (Cat# 48-0047-41, RRID:AB_1603232) or isotype control IgG (Cat# 48-

4714-80, RRID:AB_1271995), Super Bright 600 conjugated anti-CD25 (Cat# 63-0259-42, RRID:AB_2637187) or isotype control IgG (Cat# 63-4714-80, RRID:AB_2637447), peridinin chlorophyll protein (PerCp)-cyanine (Cy) 5.5 conjugated anti-CD25 (Cat# 45-0251-80, RRID:AB_914323) or isotype control IgG (Cat# 45-4301-80, RRID: AB_906256), Super Bright 645 conjugated anti-CD27 (Cat# 64-0279-42, RRID:AB_2688222) or isotype control IgG (64-4714-80, RRID:AB_2665350), phycoerythrin (PE)-Cy 7 conjugated anti-CD45RO (Cat# 25-0457-42, RRID:AB_10718534) or isotype control IgG (25-4724-81, RRID:AB_470203), APC conjugated anti-CD45RO (Cat# 17-0457-41, RRID:AB_1907398) or isotype control IgG (17-4724-81, RRID:AB_470188), APC conjugated anti-CD45RA (Cat# 17-0458-42, RRID:AB_1907398) or isotype control IgG (17-4732-81, RRID:AB_763656), fluorescein isothiocyanate (FITC) conjugated anti-CD62L (Cat# 11-0629-41, RRID:AB_10669578) or isotype control IgG (Cat# 11-4714-81, RRID:AB_470021), PE conjugated anti-CCR7 (Cat# 12-1979-41, RRID:AB_10667886) or isotype control IgG Cat# 12-4321-80, RRID:AB_1834380), and PE-Cy5.5 conjugated anti-HLA-DR (Cat# MHLDR18, RRID:AB_10372966) or isotype control IgG (Cat# 35-4732-80, RRID:AB_11218699) (all from Invitrogen). Cells were then washed in FACS buffer, then fixed and permeabilized using BD Cytofix/Cytoperm (BD Biosciences) for 30 mins at 4 °C followed by staining with APC conjugated anti-MKI67 (Cat# 17-5699-41, RRID:AB_2573217) or isotype control IgG (Cat# 17-4714-81, RRID:AB_763650) (both from Invitrogen) or PE-conjugated anti-HIV-1 core antigen (Beckman Coulter, Cat# 6604667, RRID:AB_1575989) or isotype control IgG (Invitrogen, Cat# 12-4714-42, RRID:AB_1944423) for 30 mins at 4 °C. Cells were then washed in FACS buffer before blinded acquisition using a BD Biosciences Aria II SORP flow cytometer using 405 nm laser excitation with a 605/40 BP filter to detect Super Bright 600 and a 662/15 BP filter to detect Super Bright 645, a 488 nm laser excitation with a 530/30 BP filter to detect FITC, a 585/15 BP filter to detect PE, a 680/60 BP filter to detect PE-Cy5.5, and a 705/70 BP filter to detect PerCp-Cy5.5, a 561 nm yellow/green laser and a 660/20 BP filter to detect APC and a 780/60 BP filter to detect PE-Cy7, and a 633

nm red laser with a 450/40 BP filter to detect eFluor 450 and a 780/60 BP filter to detect APC-eFluor 780. Analysis was performed using FlowJo v. 10 (BD Biosciences) using FMO and INC to determine gating strategy.

For cell death flow cytometry analysis of CD4+ T cells, 1×10^5 CD4+ T cells were harvested and stained with Alexa Fluor 488-conjugated annexin V (Cat# A13201; Thermo Fisher) and 1 µg/mL propidium iodide (Cat# P3566; Thermo Fisher) in 10 mM HEPES, 140 mM NaCl, 2.5 mM $CaCl_2$, pH 7.4 staining for 15 mins at 4 °C. Samples were then diluted 1:4 in 10 mM HEPES, 140 mM NaCl, 2.5 mM $CaCl_2$, pH 7.4 before blinded acquisition using a BD FACSCalibur flow cytometer (BD Biosciences) using the 488 nm blue laser for excitation and 530/30 BP filter for detection of Alexa Fluor 488 emission and 670/LP filter for propidium iodide. Analysis was performed using FlowJo v. 10.

LDH assay

To assess the extent of cell death, lactate dehydrogenase (LDH) activity of supernatants was measured using a mixture of diaphorase/NAD+ and 3-(4-iodophenyl)-2-(4-nitrophenyl)-5-phenyl-2H-tetrazol-3-ium chloride/sodium 2-hydroxypropanoate according to the manufacturer's protocol (Takara Bio). Staurosporine (Sigma-Aldrich Cat# S6942) was used as a control.

Cell death detection ELISA

To assess the qualitative and quantitative determination of cytoplasmic histone-associated DNA fragments (mono- and oligonucleosomes) after LCL161 or staurosporine (positive control) treatment, the Cell Death Detection ELISA was used according to the manufacturer's protocol. Enrichment factor is calculated using the following equation when mU is absorbance [10^{-3}]:

$$Enrichment\ factor = \frac{mU\ of\ the\ sample\ (dead/dying\ cells)}{mU\ of\ the\ corresponding\ control\ (viable\ cells)}$$

siRNA transfection

CD4+ T cells were transfected with Mission *BIRC2* esiRNA (ID# EHU002711) or control (Cat# EHUEGFP) siRNA (siNS) using lipofectamine RNAiMAX transfection reagent (all Invitrogen) in Opti-MEM (Gibco) according to the manufacturer's instructions. 48 h later, cells were analyzed for target gene silencing by western blot. Transfection efficiency was assessed with BLOCK-iT Alexa Fluor Red fluorescent control (Cat# 14750100, Invitrogen) using a BD FACSCalibur flow cytometer with the 488 nm blue laser for excitation and a 585/42 BP filter.

Western blotting

Cell lysis, co-immunoprecipitation, and western blotting were performed as previously described[35,49]. Briefly, cell lysates were prepared using 20 mM HEPES, 150 mM NaCl, and 1 mM EDTA supplemented with 1% Triton X-100 and 1% Thermo Scientific Halt protease and phosphatase inhibitor cocktail. Co-immunoprecipitation was performed using the Pierce Co-Immunoprecipitation Kit with 50 µg cell lysates and either 50 µg anti-FAS IgG1 (Cat# 8023, RRID:AB_10860778) with a mouse IgG1 (Cat# 5415, RRID:AB_10829607) as a negative control, or anti-RIPK1 IgG XP (Cat# 3493, RRID:AB_2305314) with a rabbit IgG XP (Cat# 3900, RRID:AB_1550038) as a negative control (all from Cell Signaling) according to the manufacturer's directions. Cell lysates and immunoprecipitates were resolved using 2-[bis(2-hydroxyethyl)amino]-2-(hydroxymethyl)propane-1,3-diol buffered polyacrylamide gels, transferred to 0.2 μm polyvinylidene difluoride membranes, probed with primary antibodies overnight at 4 °C, followed by detection using alkaline phosphatase tagged secondary antibodies (Invitrogen) and 0.25 mM CDP-Star supplemented with 5% Nitro-Block II (both Applied Biosystems). The primary antibodies raised against the following were used in western blots: BIRC2 (Cat# 7065, RRID:AB_10890862), BIRC3 (Cat# 3130, RRID:AB_10693298), cFLIP (Cat# 56343, RRID:AB_2799508), CASP3 (Cat# 14220, RRID:AB_2798429), CASP8

(Cat# 9496, RRID:AB_561381), FADD (Cat# 2782, RRID:AB_2100484), FAS (Cat# 4233, RRID:AB_2100359), FASLG (Cat# 4273, RRID:AB_2100652), PARP1 (Cat# 9532, RRID:AB_659884), RIPK1 (Cat# 3493, RRID:AB_2305314), Phospho-RIPK1-Ser166 (Cat# 44590, RRID:AB_2799268) from Cell Signaling Technologies, and ACTB (Sigma Cat# A2228, RRID:AB_476697).

REFERENCES

1 Gyrd-Hansen, M. & Meier, P. IAPs: from caspase inhibitors to modulators of NF-kappaB, inflammation and cancer. *Nature reviews. Cancer* **10**, 561-574, (2010).

2 Estornes, Y. & Bertrand, M. J. IAPs, regulators of innate immunity and inflammation. *Semin Cell Dev Biol* **39**, 106-114, (2015).

3 Mehrotra, S. *et al.* IAP regulation of metastasis. *Cancer cell* **17**, 53-64, (2010).

4 Swingler, S., Mann, A. M., Zhou, J., Swingler, C. & Stevenson, M. Apoptotic killing of HIV-1-infected macrophages is subverted by the viral envelope glycoprotein. *PLoS Pathog.* **3**, 1281-1290, (2007).

5 Wang, X., Ragupathy, V., Zhao, J. & Hewlett, I. Molecules from apoptotic pathways modulate HIV-1 replication in Jurkat cells. *Biochem. Biophys. Res. Commun.* **414**, 20-24, (2011).

6 Pache, L. *et al.* BIRC2/cIAP1 is a negative regulator of HIV-1 transcription and can be targeted by Smac mimetics to promote reversal of viral latency. *Cell Host Microbe* **18**, 345-353, (2015).

7 Zarnegar, B. J. *et al.* Noncanonical NF-kappaB activation requires coordinated assembly of a regulatory complex of the adaptors cIAP1, cIAP2, TRAF2 and TRAF3 and the kinase NIK. *Nat. Immunol.* **9**, 1371-1378, (2008).

8 Dueber, E. C. *et al.* Antagonists induce a conformational change in cIAP1 that promotes autoubiquitination. *Science* **334**, 376-380, (2011).

9 Bertrand, M. J. *et al.* cIAP1 and cIAP2 facilitate cancer cell survival by functioning as E3 ligases that promote RIP1 ubiquitination. *Molecular cell* **30**, 689-700, (2008).

10 Varfolomeev, E. *et al.* IAP antagonists induce autoubiquitination of c-IAPs, NF-kappaB activation, and TNFalpha-dependent apoptosis. *Cell* **131**, 669-681, (2007).

11 Verhagen, A. M. *et al.* Identification of DIABLO, a mammalian protein that promotes apoptosis by binding to and antagonizing IAP proteins. *Cell* **102**, 43-53, (2000).

12 Du, C., Fang, M., Li, Y., Li, L. & Wang, X. Smac, a mitochondrial protein that promotes cytochrome c-dependent caspase activation by eliminating IAP inhibition. *Cell* **102**, 33-42, (2000).

13 Vince, J. E. *et al.* IAP antagonists target cIAP1 to induce TNFalpha-dependent apoptosis. *Cell* **131**, 682-693, (2007).

14 Huang, X. *et al.* XIAP facilitates breast and colon carcinoma growth via promotion of p62 depletion through ubiquitination-dependent proteasomal degradation. *Oncogene* **38**, 1448-1460, (2019).

15 Varfolomeev, E. *et al.* c-IAP1 and c-IAP2 are critical mediators of tumor necrosis factor alpha (TNFalpha)-induced NF-kappaB activation. *The Journal of biological chemistry* **283**, 24295-24299, (2008).
16 Uren, A. G. *et al.* Role for yeast inhibitor of apoptosis (IAP)-like proteins in cell division. *Proceedings of the National Academy of Sciences of the United States of America* **96**, 10170-10175, (1999).
17 Glorian, V. *et al.* DNA damage and S phase-dependent E2F1 stabilization requires the cIAP1 E3-ubiquitin ligase and is associated with K63-poly-ubiquitination on lysine 161/164 residues. *Cell Death Dis* **8**, e2816, (2017).
18 Sauer, M. *et al.* Induction of the DNA damage response by IAP inhibition triggers natural immunity via upregulation of NKG2D ligands in Hodgkin lymphoma in vitro. *Biol Chem* **394**, 1325-1331, (2013).
19 Dogan, T. *et al.* X-linked and cellular IAPs modulate the stability of C-RAF kinase and cell motility. *Nature cell biology* **10**, 1447-1455, (2008).
20 Cartier, J. *et al.* Cellular inhibitor of apoptosis protein-1 (cIAP1) can regulate E2F1 transcription factor-mediated control of cyclin transcription. *The Journal of biological chemistry* **286**, 26406-26417, (2011).
21 Samuel, T. *et al.* cIAP1 Localizes to the nuclear compartment and modulates the cell cycle. *Cancer research* **65**, 210-218, (2005).
22 Plenchette, S. *et al.* Translocation of the inhibitor of apoptosis protein c-IAP1 from the nucleus to the Golgi in hematopoietic cells undergoing differentiation: a nuclear export signal-mediated event. *Blood* **104**, 2035-2043, (2004).
23 Fulda, S. & Vucic, D. Targeting IAP proteins for therapeutic intervention in cancer. *Nat Rev Drug Discov* **11**, 109-124, (2012).
24 Chen, S. M. *et al.* Targeting inhibitors of apoptosis proteins suppresses medulloblastoma cell proliferation via G2/M phase arrest and attenuated neddylation of p21. *Cancer Med* **7**, 3988-4003, (2018).
25 Chang, Y. C. & Cheung, C. H. An updated review of Smac mimetics, LCL161, birinapant, and CDC-0152 in cancer treatmen. *Applied Sciences* **11**, 335, (2021).
26 Fulda, S. Smac Mimetics to Therapeutically Target IAP Proteins in Cancer. *Int Rev Cell Mol Biol* **330**, 157-169, (2017).
27 Bai, L., Smith, D. C. & Wang, S. Small-molecule SMAC mimetics as new cancer therapeutics. *Pharmacol Ther* **144**, 82-95, (2014).
28 Campbell, G. R., To, R. K., Zhang, G. & Spector, S. A. SMAC mimetics induce autophagy-dependent apoptosis of HIV-1-infected macrophages. *Cell Death Dis* **11**, 590, (2020).
29 Andrews, F. H., Strahl, B. D. & Kutateladze, T. G. Insights into newly discovered marks and readers of epigenetic information. *Nature chemical biology* **12**, 662-668, (2016).
30 Musselman, C. A., Lalonde, M. E., Cote, J. & Kutateladze, T. G. Perceiving the epigenetic landscape through histone readers. *Nature structural & molecular biology* **19**, 1218-1227, (2012).
31 Taverna, S. D., Li, H., Ruthenburg, A. J., Allis, C. D. & Patel, D. J. How chromatin-binding modules interpret histone modifications: lessons from professional pocket pickers. *Nature structural & molecular biology* **14**, 1025-1040, (2007).
32 Vann, K. R., Klein, B. J. & Kutateladze, T. G. Mechanistic similarities in recognition of histone tails and DNA by epigenetic readers. *Current opinion in structural biology* **71**, 1-6, (2021).
33 Pemmaraju, N. *et al.* Final results of a phase 2 clinical trial of LCL161, an oral SMAC mimetic for patients with myelofibrosis. *Blood Adv* **5**, 3163-3173, (2021).
34 Silvestris, F. *et al.* Overexpression of Fas antigen on T cells in advanced HIV-1 infection: differential ligation constantly induces apoptosis. *AIDS* **10**, 131-141, (1996).

35 Campbell, G. R., Bruckman, R. S., Chu, Y. L., Trout, R. N. & Spector, S. A. SMAC mimetics induce autophagy-dependent apoptosis of HIV-1-infected resting memory CD4+ T cells. *Cell Host Microbe* **24**, 689-702.e687, (2018).
36 McEleny, K. *et al.* An antisense oligonucleotide to cIAP-1 sensitizes prostate cancer cells to fas and TNFalpha mediated apoptosis. *Prostate* **59**, 419-425, (2004).
37 Dynek, J. N. *et al.* c-IAP1 and UbcH5 promote K11-linked polyubiquitination of RIP1 in TNF signalling. *The EMBO journal* **29**, 4198-4209, (2010).
38 Laurien, L. *et al.* Autophosphorylation at serine 166 regulates RIP kinase 1-mediated cell death and inflammation. *Nature communications* **11**, 1747, (2020).
39 Feltham, R. & Silke, J. The small molecule that packs a punch: ubiquitin-mediated regulation of RIPK1/FADD/caspase-8 complexes. *Cell Death Differ* **24**, 1196-1204, (2017).
40 Schwarzer, R., Laurien, L. & Pasparakis, M. New insights into the regulation of apoptosis, necroptosis, and pyroptosis by receptor interacting protein kinase 1 and caspase-8. *Curr Opin Cell Biol* **63**, 186-193, (2020).
41 Campbell, G. R. *et al.* CD4+ T cell-mimicking nanoparticles encapsulating DIABLO/SMAC mimetics broadly neutralize HIV-1 and selectively kills HIV-1-infected cells. *Theranostics* **11**, 9009-9021, (2021).
42 Dupoux, A. *et al.* cIAP1-dependent TRAF2 degradation regulates the differentiation of monocytes into macrophages and their response to CD40 ligand. *Blood* **113**, 175-185, (2009).
43 Emsley, P., Lohkamp, B., Scott, W. G. & Cowtan, K. Features and development of Coot. *Acta crystallographica. Section D, Biological crystallography* **66**, 486-501, (2010).
44 Adams, P. D. *et al.* PHENIX: a comprehensive Python-based system for macromolecular structure solution. *Acta crystallographica. Section D, Biological crystallography* **66**, 213-221, (2010).
45 Kim, D., Paggi, J. M., Park, C., Bennett, C. & Salzberg, S. L. Graph-based genome alignment and genotyping with HISAT2 and HISAT-genotype. *Nat Biotechnol* **37**, 907-915, (2019).
46 Robinson, M. D., McCarthy, D. J. & Smyth, G. K. edgeR: a Bioconductor package for differential expression analysis of digital gene expression data. *Bioinformatics* **26**, 139-140, (2010).
47 Huang da, W., Sherman, B. T. & Lempicki, R. A. Systematic and integrative analysis of large gene lists using DAVID bioinformatics resources. *Nat Protoc* **4**, 44-57, (2009).
48 Tada, H., Shiho, O., Kuroshima, K., Koyama, M. & Tsukamoto, K. An improved colorimetric assay for interleukin 2. *J Immunol Methods* **93**, 157-165, (1986).
49 Velikkakath, A. K., Nishimura, T., Oita, E., Ishihara, N. & Mizushima, N. Mammalian Atg2 proteins are essential for autophagosome formation and important for regulation of size and distribution of lipid droplets. *Mol. Biol. Cell* **23**, 896-909, (2012).

Figure legends

Figure 1. BIRC2 recognizes histone tails. (a) BIRC2 domain architecture. (b) Western blot analysis of the salt gradient chromatin fractionation of SW480 nuclei. (c) Representative images of PLA (pink) between BIRC2 and histone H3 in SW480 cells. The nuclei are stained with DAPI (blue). (d) Quantification of the PLA signal in (c) with at least 75 cells analyzed per condition. Statistical analysis was performed using Wilcoxon test. (e) Western blot analysis of pull-downs of the GST-tagged BIR domains of BIRC2 with the indicated histone peptides. RBP2-PHD, control. (f) Superimposed $^{1}H,^{15}N$ HSQC spectra of ^{15}N-labeled BIR domains of BIRC2, collected while the $H3_{1-12}$ peptide was titrated in the NMR samples. Spectra are color coded according to the protein:peptide molar ratio. (g, h) Representative binding curves used to determine K_ds by tryptophan fluorescence. The K_d values were averaged over three separate experiments, with error calculated as standard deviation between the runs. (i) Electrostatic surface potential of $BIRC2_{BIR3}$ is colored blue and red for the positive charge and the negative charge, respectively. The bound H3 peptide is shown as yellow sticks. (j, k) A ribbon diagram of the $BIRC2_{BIR3}$ (green) in complex with the histone H3 peptide (yellow). Dashed lines represent hydrogen bonds. The zinc ion is shown as a grey sphere.

Figure 2. BIRs mediate histone and DNA binding functions of BIRC2. (a, b) Western blot analysis of pull-downs of the GST-tagged BIR domains of BIRC2 with the indicated histone peptides. RBP2-PHD, control. (c, d) Overlays of $^{1}H,^{15}N$ HSQC spectra of the BIR domains of BIRC2 collected before (black) and after addition of the indicated peptides. Spectra are color coded according to the protein:peptide molar ratio. (e-g) Overlays of $^{1}H,^{15}N$ HSQC spectra of the mutated BIRC2 BIR domains collected before (black) and after addition of the indicated peptides. Spectra are color coded according to the protein:peptide molar ratio. (h, i) Western blot analysis of pull-downs of the GST-tagged mutated BIRC2 BIR domains with the indicated histone peptides. (j) Alignment of a fragment of the amino acid sequences of the BIRC2 BIR

752 domains. Identical residues are highlighted by red boxes and moderately conserved residues
753 are colored red. $BIRC2_{BIR3}$ residues are labeled. (k-m) EMSAs of 147 bp 601 DNA in the
754 presence of increasing amounts of the indicated BIR domains of BIRC2. DNA:protein ratio is
755 shown below gel images.
756
757 **Figure 3. BIRC2 mediates the cell defense and cell cycle signaling.** (a) Heatmap of
758 common differentially expressed genes (DEGs) in MCF7 cells treated with BIRC2 sgRNAs or
759 the control GFP sgRNA. Genes are shown as Z-score $\log_2$ CPM (counts per million reads
760 mapped). Up-regulated genes are shown in red and down-regulated genes in blue. (b) Top
761 ranked Gene Ontology (GO) biological process terms of up (red) and down (blue) regulated
762 genes of DEGs as in (a) in BIRC2 KO cells. The full lists are shown in Suppl. Tables 2 and 3. (c)
763 A cytokines antibody array with supernatants derived from human macrophages obtained by *ex-*
764 *vivo* differentiation of normal blood monocytes and stimulated with IFN-γ for 24 h in the
765 presence of 10 μM embelin or vehicle as control. (d-f) HeLa cells transfected with either BIRC2-
766 encoding of empty vector were untreated (NT) or treated with 1 μM etoposide (eto) for 3 h (0),
767 then washed and incubated for 2 to 45 h in a drug-free medium. Western blot analysis of BIRC2
768 and the loading control HSC70 is shown in (d). Western blot analysis of γH2AX, a mark of DNA
769 damage, in untreated cells (NT) or etoposide treated cells that were washed and incubated for
770 additional 2 or 6 h in an etoposide-free medium is shown in (e). Flow cytometry analysis of
771 γH2AX in untreated cells (NT, grey histograms) or etoposide treated cells that were washed and
772 incubated for additional 2 or 6 h in an etoposide-free medium (eto, red histograms) is shown in
773 (f). The percentage of cells expressing γH2AX is indicated. (g) Flow cytometry analysis of the
774 cell cycle in etoposide treated HeLa cells that were incubated for indicated time in an etoposide-
775 free medium. DNA was stained with Propidium iodide. (h) % of cells in G2/M. Data represent
776 mean ± SEM from three independent biological replicates for 24, 30 and 48 hrs and two for 45
777 hrs (the unpaired t-test per row in GraphPad Prism).

Figure 4. LCL161 binds to BIRC2$_{BIR2}$ and BIRC2$_{BIR3}$. (a) Chemical structure of LCL161. (b-d) Superimposed $^{1}H,^{15}N$ HSQC spectra of ^{15}N-labeled BIRC2$_{BIR1}$, BIRC2$_{BIR2}$ and BIRC2$_{BIR3}$, collected while LCL161 was titrated in the NMR samples. Spectra are color coded according to the protein:inhibitor molar ratio. (e, f) Representative binding curves used to determine K_ds by tryptophan fluorescence. The K_d values were averaged over three separate experiments, with error calculated as standard deviation between the runs. (g) Electrostatic surface potential of BIRC2$_{BIR3}$ is colored blue and red for the positive charge and the negative charge, respectively. The bound LCL161 compound is shown as green sticks. (h) A ribbon diagram of the BIRC2$_{BIR3}$ (wheat) in complex with LCL161 (green). Dashed lines represent hydrogen bonds. The zinc ion is shown as a grey sphere. (i) Structural overlay of BIRC2$_{BIR3}$ bound to LCL161 (green) and the H3 peptide (yellow). (j) Superimposed LCL161 (green) and the H3 peptide (yellow) bound to BIRC2$_{BIR3}$.

Figure 5. LCL161 disrupts binding of BIRC2 to H3 and induces cell death. (a) Representative images of the PLA between BIRC2 and histone H3 in SW480 cells treated with or without 10 μM LCL161 for 1 h. The nuclei were stained with DAPI (blue). (b) Quantification of the PLA signal in (a) with at least 75 cells analyzed per condition. Statistical analysis was performed using Wilcoxon test. (c) Western blot analysis of peptide pull-downs of GST-tagged BIRC2$_{BIR3}$ with the histone H3 peptide (aa 1-22) in the presence of increasing concentrations of LCL161. (d) Western blot analysis of BIRC2 in SW480 cells treated with or without 10 μM LCL161 for 1 h. β-Actin was used as loading control. (e) Western blot analysis of BIRC2 in human macrophages obtained by *ex-vivo* differentiation of normal blood monocytes and stimulated or non-stimulated with IFN-γ for 24 h in the presence or absence of 10 μM LCL161. β-Actin was used as loading control. (f, g) RT-qPCR analysis of IL-6 (f) and RANTES (g) mRNA

803 expression levels in human macrophages stimulated or non-stimulated with IFN-γ for 24 h in the
804 presence or absence of 10 μM LCL161. Data represent mean ± SD of four independent
805 experiments (the paired t-test in GraphPad Prism). * P<0.05; ** P<0.01. (h, i) MTT assay
806 showing survival of murine MEF (h) or human glioma LN18 cells (i) incubated for 24 h in media
807 containing the indicated concentrations of LCL161 and/or TNFα. Data represent mean ± SEM
808 from three independent biological replicates. (j) Representative western blots of FAS,
809 membrane-bound FASLG (mFASLG), soluble FASLG (sFASLG), BIRC2, and BIRC3 in
810 uninfected CD4+ T cells (T_{CM}) and HIV-1-infected CD4+ T cells (HIV-T_{CM}). n = 4. (k) T_{CM} and
811 HIV-T_{CM} were treated with 100 nM LCL161 for 4 h. FAS was immunoprecipitated using anti-FAS
812 with a mouse IgG1 (α-IgG as a negative control). Immunoprecipitates and cell lysates were
813 analyzed by western blot using the indicated antibodies. n = 4. (l) T_{CM} and HIV-T_{CM} were treated
814 with 100 nM LCL161 for 5 min. RIPK1 was immunoprecipitated using anti-RIPK1 with a rabbit
815 IgG (α-IgG) as a negative control, and endogenous RIPK1 ubiquitination detected by western
816 blotting using an RIPK1 antibody. n = 4. (m) T_{CM} and HIV-T_{CM} were treated with 100 nM LCL161
817 for 4 h. Cell lysates were analyzed by western blot using the indicated antibodies. n = 4. (n) T_{CM}
818 and HIV-T_{CM} were treated with LCL161 or 2 μM staurosporine (STS) for 4 h. *Top,* aliquots of
819 supernatants were spectrophotometrically tested for LDH as a measure of cell death. *Bottom,*
820 cells were harvested and cytoplasmic fractions assayed for cytoplasmic histone-associated
821 DNA fragments (mono- and oligonucleosomes) by ELISA (see Methods for calculation of
822 enrichment factor). n = 4.
823
824
825
826 **Supplementary Table 2.** CPM values for all expressed genes.
827 **Supplementary Table 3.** Gene Ontology biological process terms of DEGs in BIRC2 KO cells.

Figure 1

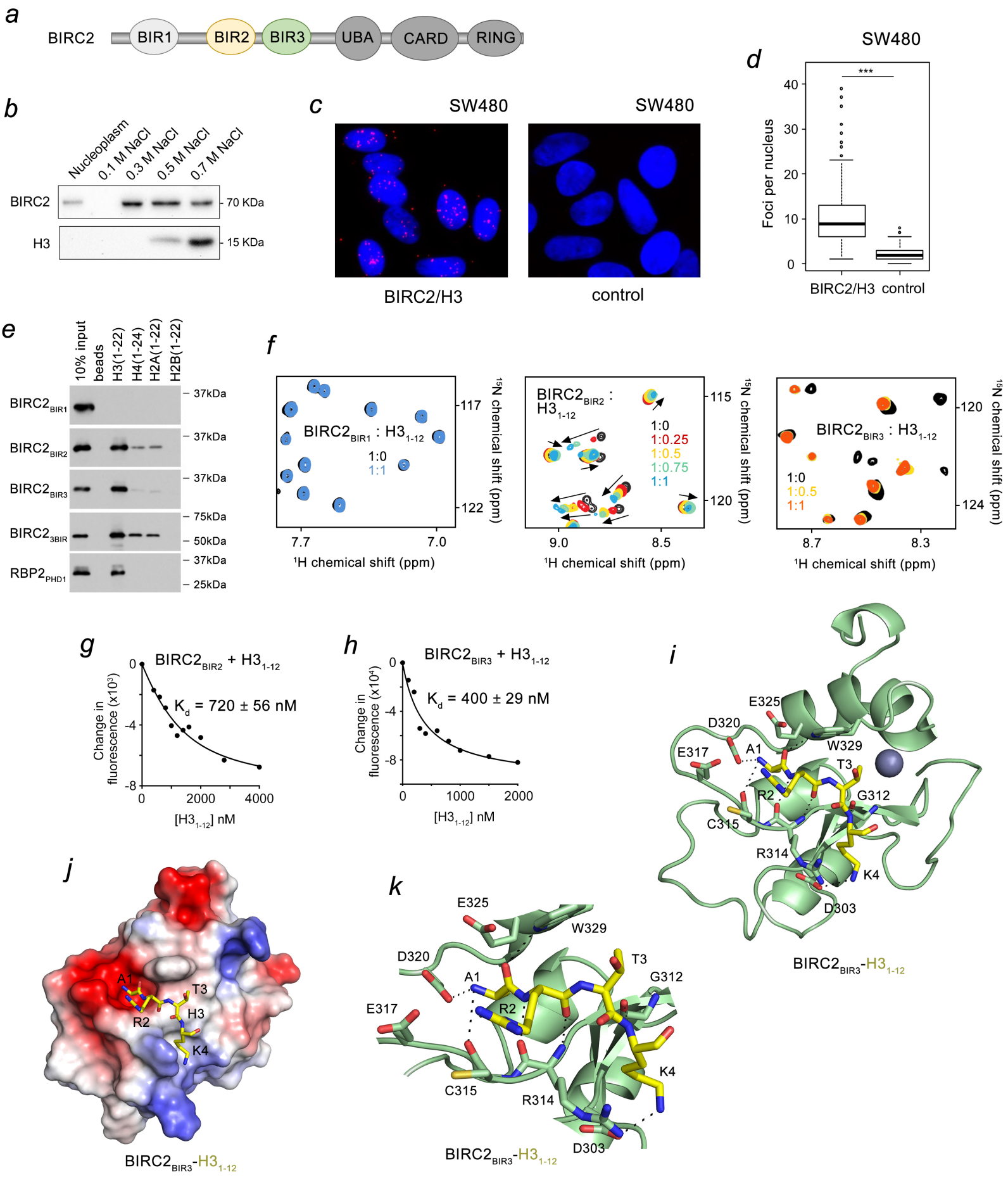
a
BIRC2
BIR1
BIR2
BIR3
UBA
CARD
RING
b
Nucleoplasm
0.1 M NaCl
0.3 M NaCl
0.5 M NaCl
0.7 M NaCl
BIRC2
70 KDa
H3
15 KDa
c
SW480
SW480
BIRC2/H3
control
d
SW480
***
Foci per nucleus
BIRC2/H3
control
e
10% input
beads
H3(1-22)
H4(1-24)
H2A(1-22)
H2B(1-22)
BIRC2BIR1
37kDa
BIRC2BIR2
37kDa
BIRC2BIR3
37kDa
BIRC2 3BIR
75kDa
50kDa
RBP2PHD1
37kDa
25kDa
f
BIRC2BIR1 : H3 1-12
1:0
1:1
BIRC2BIR2 : H3 1-12
1:0
1:0.25
1:0.5
1:0.75
1:1
BIRC2BIR3 : H3 1-12
1:0
1:0.5
1:1
15N chemical shift (ppm)
1H chemical shift (ppm)
g
BIRC2BIR2 + H3 1-12
Kd = 720 ± 56 nM
Change in fluorescence (x10³)
[H3 1-12] nM
h
BIRC2BIR3 + H3 1-12
Kd = 400 ± 29 nM
Change in fluorescence (x10⁴)
[H3 1-12] nM
i
E325
D320
E317
A1
W329
T3
R2
G312
C315
R314
K4
D303
BIRC2BIR3-H3 1-12
j
A1
T3
R2
H3
K4
BIRC2BIR3-H3 1-12
k
E325
W329
D320
T3
A1
G312
E317
R2
K4
C315
R314
D303
BIRC2BIR3-H3 1-12

Figure 2

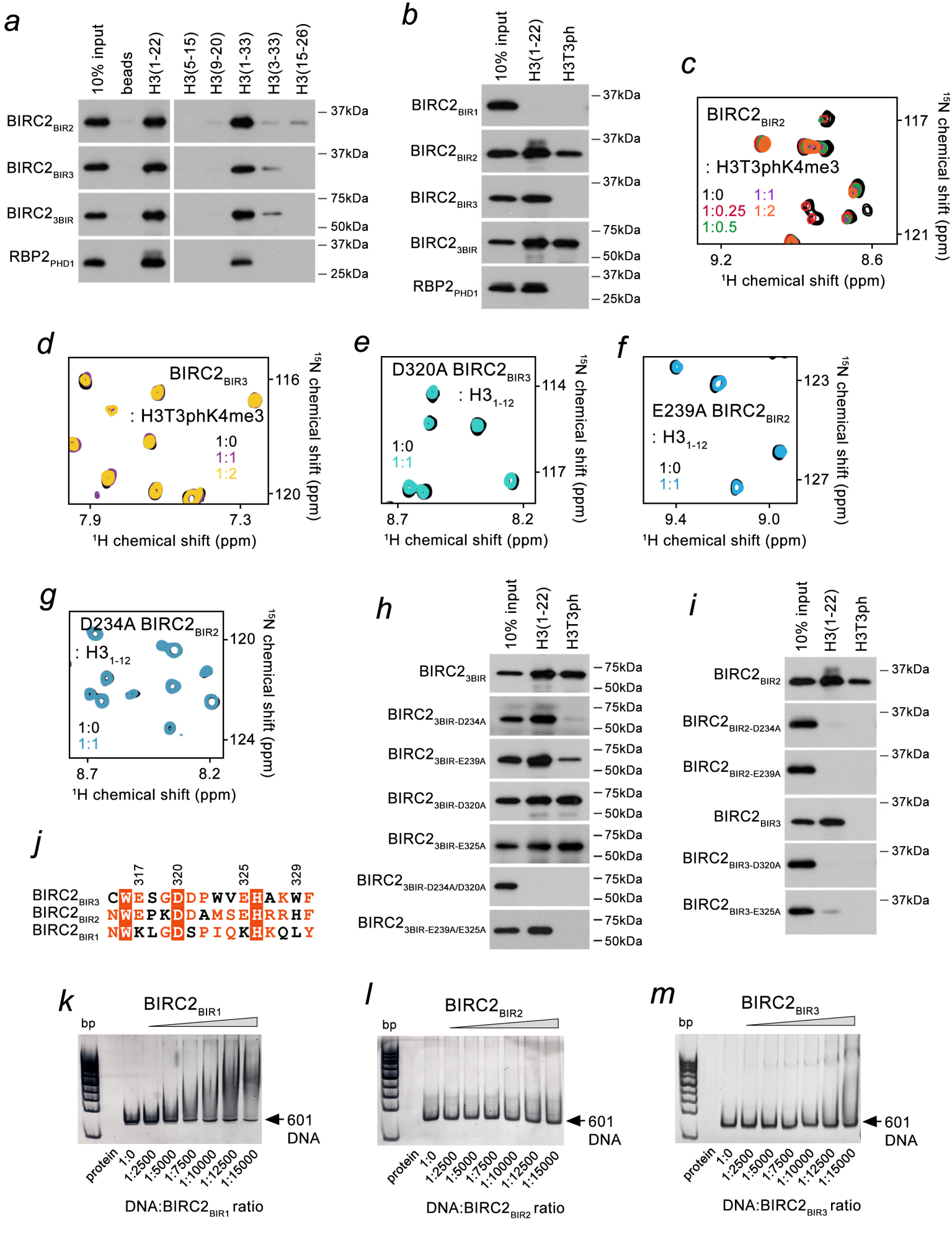
a
10% input
beads
H3(1-22)
H3(5-15)
H3(9-20)
H3(1-33)
H3(3-33)
H3(15-26)
BIRC2BIR2
BIRC2BIR3
BIRC2 3BIR
RBP2PHD1
37kDa
75kDa
50kDa
25kDa
b
10% input
H3(1-22)
H3T3ph
BIRC2BIR1
BIRC2BIR2
BIRC2BIR3
BIRC2 3BIR
RBP2PHD1
c
BIRC2BIR2
: H3T3phK4me3
1:0
1:0.25
1:0.5
1:1
1:2
15N chemical shift (ppm)
1H chemical shift (ppm)
d
BIRC2BIR3
: H3T3phK4me3
1:0
1:1
1:2
e
D320A BIRC2BIR3
: H31-12
1:0
1:1
f
E239A BIRC2BIR2
: H31-12
1:0
1:1
g
D234A BIRC2BIR2
: H31-12
1:0
1:1
h
10% input
H3(1-22)
H3T3ph
BIRC2 3BIR
BIRC2 3BIR-D234A
BIRC2 3BIR-E239A
BIRC2 3BIR-D320A
BIRC2 3BIR-E325A
BIRC2 3BIR-D234A/D320A
BIRC2 3BIR-E239A/E325A
i
10% input
H3(1-22)
H3T3ph
BIRC2BIR2
BIRC2BIR2-D234A
BIRC2BIR2-E239A
BIRC2BIR3
BIRC2BIR3-D320A
BIRC2BIR3-E325A
j
317
320
325
329
BIRC2BIR3 CWESGDDPWVEHAKWF
BIRC2BIR2 NWEPKDDAMSEHRRHF
BIRC2BIR1 NWKLGDSPIQKHKQLY
k
BIRC2BIR1
bp
601 DNA
protein
1:0
1:2500
1:5000
1:7500
1:10000
1:12500
1:15000
DNA:BIRC2BIR1 ratio
l
BIRC2BIR2
bp
601 DNA
DNA:BIRC2BIR2 ratio
m
BIRC2BIR3
bp
601 DNA
DNA:BIRC2BIR3 ratio

Figure 3

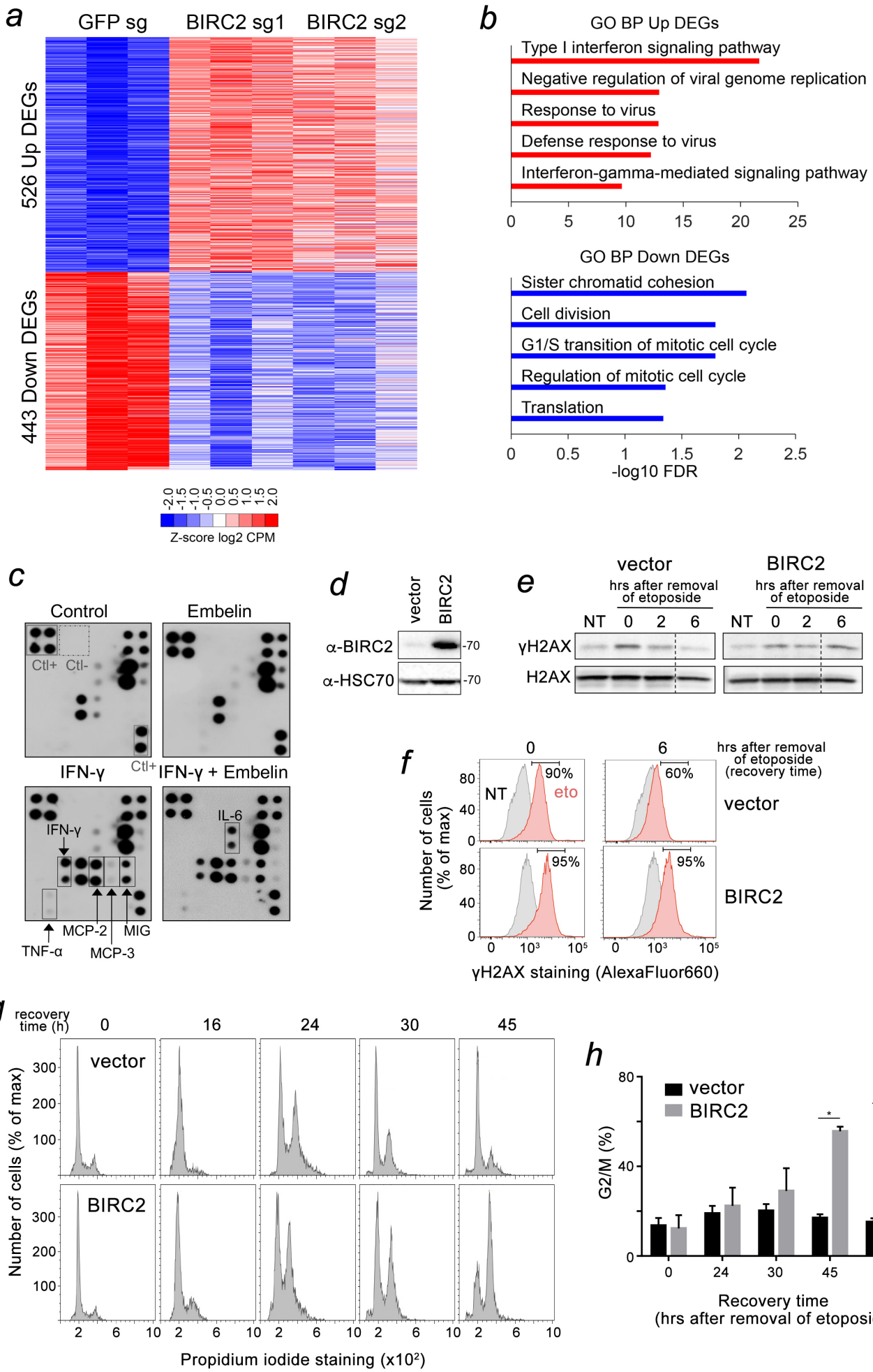
a
GFP sg
BIRC2 sg1
BIRC2 sg2
526 Up DEGs
443 Down DEGs
-2.0 -1.5 -1.0 -0.5 0.0 0.5 1.0 1.5 2.0
Z-score log2 CPM
b
GO BP Up DEGs
Type I interferon signaling pathway
Negative regulation of viral genome replication
Response to virus
Defense response to virus
Interferon-gamma-mediated signaling pathway
0 5 10 15 20 25
GO BP Down DEGs
Sister chromatid cohesion
Cell division
G1/S transition of mitotic cell cycle
Regulation of mitotic cell cycle
Translation
0 0.5 1 1.5 2 2.5
-log10 FDR
c
Control
Embelin
Ctl+
Ctl-
Ctl+
IFN-γ
IFN-γ + Embelin
IL-6
IFN-γ
MCP-2
MIG
TNF-α
MCP-3
d
vector
BIRC2
α-BIRC2
α-HSC70
-70
-70
e
vector
BIRC2
hrs after removal of etoposide
NT 0 2 6
NT 0 2 6
γH2AX
H2AX
f
0
6
hrs after removal of etoposide (recovery time)
90%
eto
NT
60%
vector
95%
95%
BIRC2
Number of cells (% of max)
γH2AX staining (AlexaFluor660)
g
recovery time (h)
0 16 24 30 45
vector
BIRC2
Number of cells (% of max)
Propidium iodide staining (x10²)
h
vector
BIRC2
G2/M (%)
0 24 30 45 48
Recovery time (hrs after removal of etoposide)

Figure 4

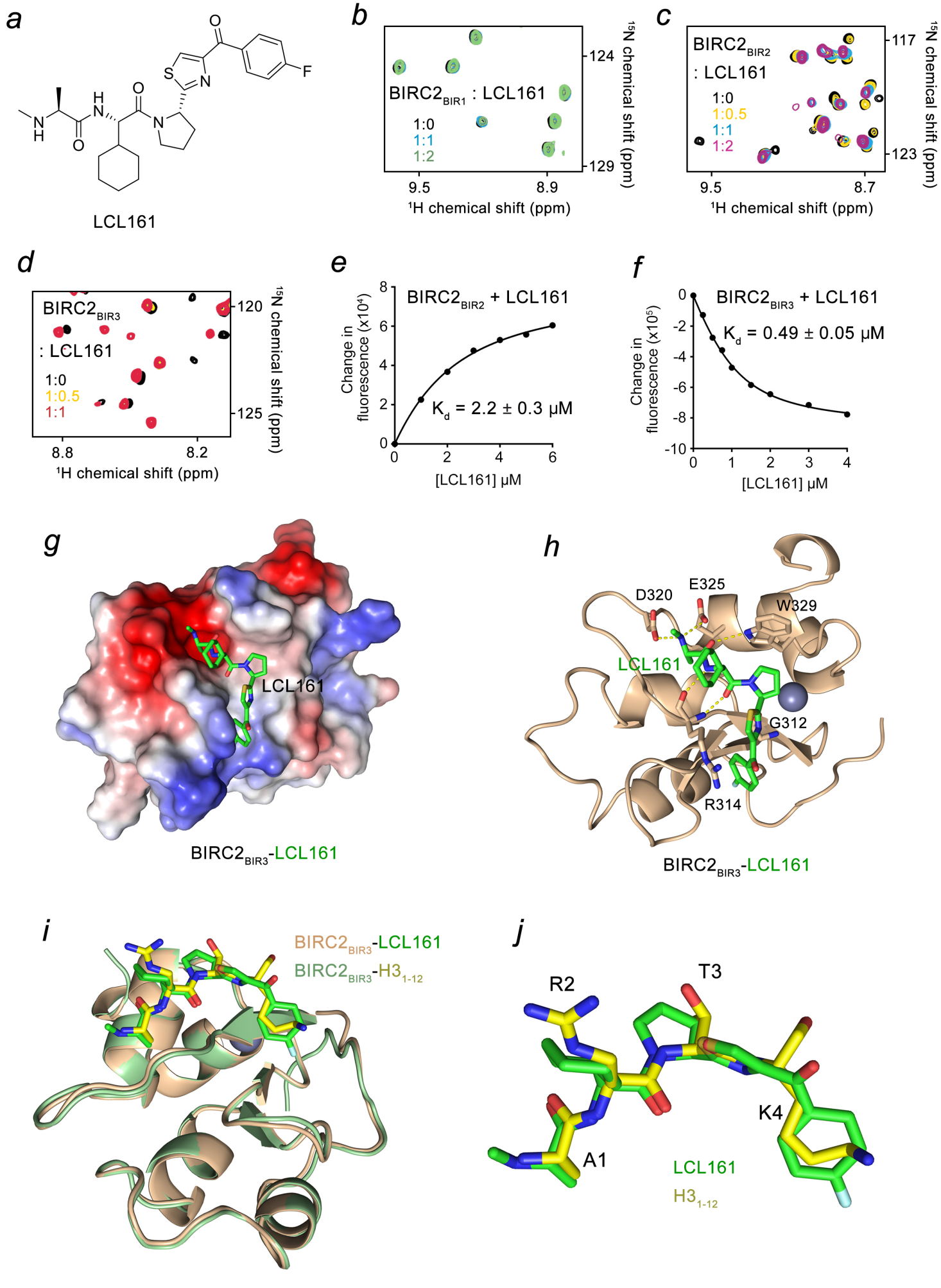
a
LCL161
b
BIRC2BIR1 : LCL161
1:0
1:1
1:2
124
129
15N chemical shift (ppm)
9.5
8.9
1H chemical shift (ppm)
c
BIRC2BIR2
: LCL161
1:0
1:0.5
1:1
1:2
117
123
15N chemical shift (ppm)
9.5
8.7
1H chemical shift (ppm)
d
BIRC2BIR3
: LCL161
1:0
1:0.5
1:1
120
125
15N chemical shift (ppm)
8.8
8.2
1H chemical shift (ppm)
e
BIRC2BIR2 + LCL161
Change in fluorescence (x10^4)
Kd = 2.2 ± 0.3 μM
[LCL161] μM
f
BIRC2BIR3 + LCL161
Change in fluorescence (x10^5)
Kd = 0.49 ± 0.05 μM
[LCL161] μM
g
LCL161
BIRC2BIR3-LCL161
h
D320
E325
W329
LCL161
G312
R314
BIRC2BIR3-LCL161
i
BIRC2BIR3-LCL161
BIRC2BIR3-H31-12
j
R2
T3
K4
A1
LCL161
H31-12

Figure 5

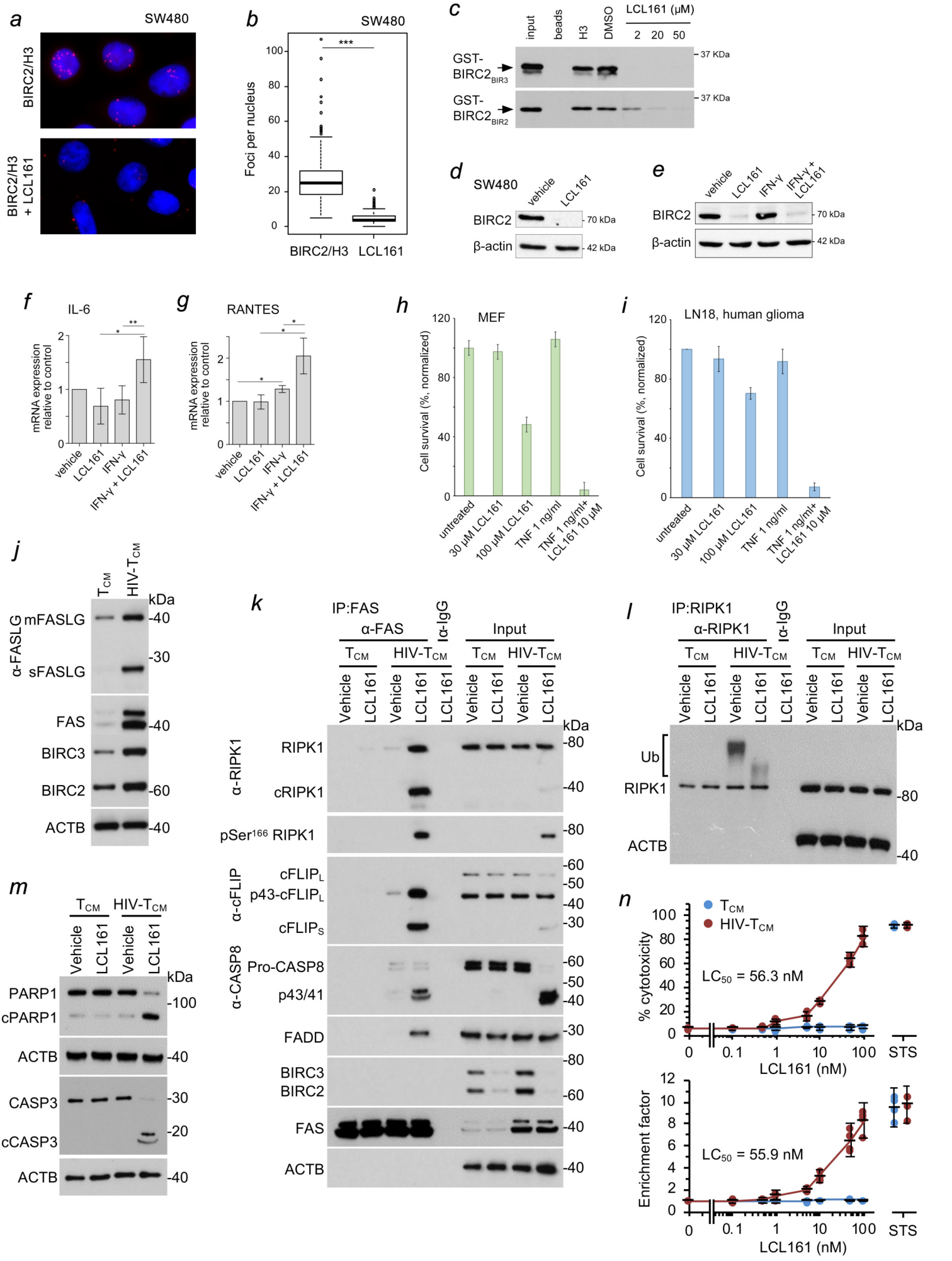
a
SW480
BIRC2/H3
BIRC2/H3 + LCL161
b
SW480
Foci per nucleus
***
BIRC2/H3
LCL161
c
input
beads
H3
DMSO
LCL161 (μM)
2 20 50
GST-BIRC2BIR3
GST-BIRC2BIR2
37 KDa
d
SW480
vehicle
LCL161
BIRC2
β-actin
70 kDa
42 kDa
e
vehicle
LCL161
IFN-γ
IFN-γ + LCL161
f
IL-6
mRNA expression relative to control
g
RANTES
h
MEF
Cell survival (%, normalized)
untreated
30 μM LCL161
100 μM LCL161
TNF 1 ng/ml
TNF 1 ng/ml+ LCL161 10 μM
i
LN18, human glioma
j
TCM
HIV-TCM
kDa
α-FASLG
mFASLG
sFASLG
FAS
BIRC3
BIRC2
ACTB
k
IP:FAS
α-FAS
α-IgG
Input
Vehicle
LCL161
α-RIPK1
RIPK1
cRIPK1
pSer166 RIPK1
α-cFLIP
cFLIPL
p43-cFLIPL
cFLIPS
α-CASP8
Pro-CASP8
p43/41
FADD
l
IP:RIPK1
α-RIPK1
Ub
m
PARP1
cPARP1
CASP3
cCASP3
n
% cytotoxicity
LC50 = 56.3 nM
LCL161 (nM)
STS
Enrichment factor
LC50 = 55.9 nM